

# Harmonic Deflections of an Infinite Floating Plate

Colin Fox and Hyuck Chung

## Abstract

As a model for a homogeneous sheet of floating sea-ice undergoing periodic vertical loading, we treat the case of an infinite thin plate floating on a fluid of constant depth. We derive the vertical deflection of the floating plate resulting from harmonic forcing at a point and along a line. These correspond to the Green's functions for forcing of a floating plate and floating beam, respectively. For finite water depths the solutions are written as series which are readily summable. When the fluid depth is large, or infinite, the solutions simplify to a sum of special functions, summed over three roots of a fifth-order polynomial. A non-dimensional formulation is given that reduces the results to a few canonical solutions corresponding to distinct physical regimes. Properties of the non-dimensional formulation are discussed.

## Contents

1	Introduction . . . . .	2
1.1	Preview . . . . .	2
1.2	Historical review . . . . .	3
2	The Green's function . . . . .	7
2.1	Mathematical model . . . . .	7
2.2	Non-dimensional formulation . . . . .	8
2.2.1	Point and line forcing . . . . .	9
2.3	Spatial Fourier transform . . . . .	9
2.3.1	Response to wave-like forcing . . . . .	10
2.4	Harmonic forcing . . . . .	11
2.4.1	Dispersion equation . . . . .	11
2.5	Inverse Fourier transform . . . . .	11
2.5.1	Residues of $\eta(k)$ . . . . .	13
2.6	Summary of calculating the Green's function . . . . .	13
2.7	Description of modes . . . . .	14
3	Response in special cases . . . . .	15
3.1	Deflection for deep water . . . . .	15
3.2	Deflection at the location of forcing . . . . .	17
3.2.1	Deflection at the point of forcing . . . . .	18
3.2.2	Deflection on the line of forcing . . . . .	20
3.2.3	Deep water . . . . .	20

3.3	Deflection and strain near to point forcing . . . . .	22
3.4	Far-field deflection . . . . .	23
3.5	Static forcing . . . . .	23
4	Properties of the non-dimensionalization . . . . .	24
4.1	Canonical solutions . . . . .	26
4.2	Other scalings . . . . .	28
4.3	The approximation $m = 0$ . . . . .	28
5	Conclusions . . . . .	30

# 1 Introduction

The New Zealand Programme in Sea-Ice Studies has a long standing interest in the coupling of ocean waves to shore-fast ice, and the resulting fatigue that produces break-up and other phenomena of geophysical importance [1, 7, 8]. That coupling is completely determined once the propagation of waves (including non-travelling waves) is characterized in the open sea and ice covered sea. Since the propagation of ocean waves is well understood, our interest turns to characterizing wave propagation in an ice cover.

As a first step towards theoretically determining the large-scale propagation characteristics of actual heterogeneous sea ice, we derive the Green’s function for local forcing of an infinite homogeneous ice cover. It is intended that this “free-space” fundamental solution will be used within a boundary-integral formulation to express the propagation through a composite ice cover consisting of locally homogeneous pieces of ice joined by cracks, pressure ridges, steps in thickness, and other types of transitions. Ice features that are strip-like are treated by considering the response to forcing on a line, while the more general case it treated by deriving the response to forcing at a point. These responses are the Green’s functions for a floating beam and floating plate, respectively.

The Green’s function models the response of a uniform sheet of fast ice when locally loaded at rates at which the ice may be taken to be elastic. Thus, the response to harmonic point forcing also enables the design and interpretation of field measurements in which surface gradient is measured generated by local harmonic loading. Using the Green’s function, we are able to calculate the effective mechanical properties of the ice sheet over scales of interest. This technique is currently being developed in field tests being undertaken in McMurdo Sound, Antarctica.

## 1.1 Preview

The central result presented here is the derivation in section 2 of the Green’s function in non-dimensional form for harmonic forcing at a point and along a line. The derivation uses the spatial Fourier transform of the governing equations with the inverse transform found analytically and written as a sum over natural modes of a floating plate. A summary of the calculations required is given in subsection 2.6. In section 3 we derive simplified forms of the Green’s functions for special geometries of typical interest. The deflection in the case of deep water is given in subsection

3.1. In that regime the influence of water depth is minimized and consequently that geometry is useful in experimental work. The calculations required to evaluate the Green’s function are greatly simplified when the water is deep because the integral over the continuum of evanescent modes can be performed analytically. The cases of measuring deflection at the location of forcing, and far from the forcing, are treated in subsections 3.2 and 3.4. The nondimensionalization used is discussed in section 4. We show that the physical behaviour is separated into the two basic physical regimes of quasi-static and dynamic responses, with maximum coupling occurring in the transition between these regimes. The response within each of these regimes is graphed in subsection 4.1. The validity of neglecting the mass of the ice sheet is examined in subsection 4.3 as this approximation is used by many authors and removes any geometry-related coefficients from the non-dimensional solutions. We observe that the approximation does not qualitatively change solutions, but gives sufficient quantitative change so that mass density needs to be included when interpreting measurements.

## 1.2 Historical review

The mathematical investigation of the vibration of plates on foundations of various types and of motion at fluid surfaces has been of long standing interest, with many mathematical developments motivated by these studies. Our study of a thin plate vibrating on a fluid foundation draws on previous investigations and most of the mathematical steps we take can be seen in earlier papers. We will not attempt to survey the vast literature on the subject but, rather, highlight the key papers that have influenced this work.

For the purpose of studying the vibration of floating sea ice it suffices to consider the linearized form of the governing equations. While the, primarily geometric, nonlinear terms in a more complete model make a quantitative difference at non-infinitesimal amplitudes [3, 4], it has been found that the difference is not significant at displacements and strains below those that cause the ice to break [6]. For such linear systems, the rationale of studying forcing at a point is well established since once the response is known the motion due to any distribution of forces may be calculated using linear superposition. This is expressed mathematically by the response to point forcing giving the kernel of an integral transform that is the inverse of the governing differential equations [32]. In general the integral transform is given by Green’s theorem for the boundary value problem and the kernel is a fundamental solution or, more specifically, a Green’s function if it also satisfies the homogeneous form of the boundary conditions. In our case those boundary conditions are Sommerfeld type radiation conditions at infinity, in which case the response is more usually referred to as the “free-space” fundamental solution, taking the name from electrostatics where this type of solution was studied. To avoid possible confusion, it should be noted that we do not actually assert Sommerfeld-type radiation conditions in this paper, preferring instead to introduce damping which causes any finite field at infinity to have no influence. In shift-invariant systems, such as when considering an infinite homogeneous sheet of ice, the integral transform simplifies to a convolution.

Linear time invariant systems, such as the title problem, are common in electrical engineering where the causal fundamental solution [32] is called the *impulse response* [18]. The Fourier transform of the impulse response is called the transfer function and characterizes the response of the system to input of the form  $\exp\{i\omega t\}$  which is an eigenfunction of such systems. Hence each solution presented here can be seen as the spatially-dependent transfer function from the applied forcing to any point on the ice sheet.

Wave propagation through ice covered seas was studied theoretically as early as 1887 by Greenhill [10] who introduced the use of the thin elastic plate as the surface boundary condition modelling the influence of the ice sheet. His study predicted, for example, that the dispersion of surface flexural-gravity waves within an ice cover differs from the dispersion of surface waves in open water. Although the Young's modulus of actual ice sheets varies significantly through the thickness – primarily due to the gradient in temperature – the use of a homogeneous plate model was established theoretically in 1972 by Kerr and Palmer [11] who showed that the elastic response can be accurately modelled using a homogeneous plate with a modified, effective, flexural rigidity. While profound advances have been made in plate theory, particularly in Mindlin's 1951 [12] paper, Fox showed that terms associated with thick-plate models such as transverse shear and rotational inertia are negligible at periods and wavelengths of geophysical interest for even very thick ice sheets [5]. The use of a thin plate model for sea ice has also been validated by field measurements. For example, Squire, Rottier and Fox [23] made measurements of the surface strain generated by ocean waves near the edge of shore-fast sea ice and found that specific details predicted using the thin plate model were visible in the strain records.

Several years prior to Greenhill's work, Hertz made a theoretical study of infinite fluid-loaded plates and in 1884 [15] published the solution for the static problem of a floating infinite plate with a load concentrated at the origin. He wrote the solution as an infinite series and was able to calculate that solution sufficiently to make the intriguing observation that it is possible to have a thin disc that would sink when unloaded, but float with an appropriate weight placed at its centre. In this static case, the fluid support of the plate is due to the buoyancy term only, and hence is the same as a Winkler foundation in which the restoring force is proportional to displacement. Hertz' solution was used by Westergaard in 1926 [22] to calculate the deflections and stresses in concrete road slabs resulting from wheel loads for the purpose of highway design. Westergaard's paper contains detailed graphs of Hertz' solution, taking advantage of the tables of Bessel functions available at the time. This static solution is usually associated with the name of Wyman who, in 1950 [36], obtained the same solution for a concentrated static load in terms of a single Kelvin function, apparently unaware of the earlier work. Wyman gave his solution in nondimensional form by scaling length with respect to the characteristic length of the ice sheet, using the same definition that we find useful in this paper.

When the loading is sufficiently slow that only the buoyancy force in the fluid support is significant, or is static as mentioned above, the fluid foundation reduces to the simpler case of a Winkler foundation. Despite there being no justification for the Winkler foundation being a suitable model for the foundation of floating ice away

from the static regime, that approximation has been used to model the dynamics of floating ice, and, as observed by Dempsey, et al. [28] has been used in geophysics and ice engineering in spite of known limitations. Standard solutions in the form of an integral transform were given for time-dependant response of a forced beam, and plate, on a Winkler foundation by Stadler and Shreeves [24], and Stadler [25], respectively, the latter containing a delightful history of the mathematical models and solutions. These papers used the same method of solution as that developed earlier by Sneddon [26, 27] for solving problems of this type, when he derived the time-dependent responses of thin plates and various foundations, separately. Sneddon's method ([27] chapter 4) uses the Fourier transform to write the governing differential equations as a second-order initial-value problem for each Fourier component (cf. our Eqn. 12) and then writes the solution of that equation as the (temporal) convolution of the forcing term with the causal fundamental solution of the differential equation, leaving that calculation and the required inverse (spatial) Fourier transform to be performed for specific loadings  $p_a(x, y, t)$ . Our approach, in contrast, is to focus on forcing with harmonic time dependence and actually perform the inverse Fourier transform. Sneddon's method was also used by Dempsey and Zhao [30], and Zhao and Dempsey [29] who studied the forced motion of floating ice sheets using a model that encompassed both fluid and Winkler foundations and concluded that Winkler foundation with added mass did not model the dynamic response accurately as the required added mass term varied with space and time.

Fritz John gave the earliest complete analysis of displacement at the surface of a heavy inviscid irrotational liquid, in a pair of excellent papers in 1949/50 [16, 17]. In the second of these John gave an expression for the motion of finite depth water excited by a harmonic point source at an arbitrary position in the water. He used that Green's function within a boundary integral formulation to solve for the wave scattering from floating bodies. The solutions were written as a sum over modes, with modal frequencies given by the roots of a transcendental (dispersion) equation and with coefficients expressed as a smooth, rational polynomial, of modal wave number. This anticipates the route that we find productive here. In particular, John discusses the complete countably infinite set of evanescent modes that are required for the solution, thereby improving on a number of papers that followed. For work that predates distribution theory these papers are remarkably easy to place in a modern context, and provide expressions that are simple to evaluate with present computational tools. Ten years after John's work, Wehausen and Laitone in their classic paper [40] derived the velocity potential for the same problem with infinite depth water. In that case the evanescent modes form a continuum, which they included and developed the solution to a form suitable for efficient computation.

Forced motion of a thin elastic plate at the surface of a liquid, i.e. the title problem, has been studied by a number of authors previously, the majority of whom have considered harmonic forcing and then employed the Fourier transform to reduce the problem to an algebraic system which can be solved to give an expression for the displacement in terms of an inverse Fourier transform. Apart from a few niceties, that is the also the basic analysis used in this paper. Our contribution is to show that by understanding the structure of the roots of the dispersion equation that inverse

transform may be performed giving the solution as a sum over modes which is simple to evaluate and also makes clear the regimes of canonical physical behaviour of the system. Both stationary and moving loading has been considered, we focus on the former and note that formally a moving load may be treated as the superposition of stationary harmonic loads. To date, authors have either simply given the expression for the inverse Fourier transform or evaluated the transform numerically for a particular force. An early example is due to Kheisin who, in 1967 ([19] chapter 4), derived the inverse transform in physical variables and determined some properties of the response in the simplifying cases of shallow water and static forcing. It is interesting to note that Kheisin scaled length in his solution using the characteristic length, as we do, but used the strange choice of the bobbing frequency of a buoy to scale time. Kheisin was aware of the more fundamental characteristic frequency that we use here, giving a definition for “critical frequency” based on the coincidence of group and phase speeds. In 1970, Nevel [13] extended that derivation to treat the case of harmonic forcing on a circle of radius  $R$ , with the solution scaled using characteristic length and time as we use here, and numerically computed the inverse for the case  $R = 0$ , i.e. point loading, at the location of the forcing. One advance made in this paper is to give a simple expression (our equation 41) for the result computed by Nevel. In 1991 Duffy [34] calculated the response of floating ice to a moving, vibrating, line load by transforming in space and time, as we do here, and wrote the inverse spatial transform as a sum over exponential modes with wavenumbers given by the roots of the dispersion equation. The temporal, Laplace, transform was inverted numerically to give the solutions in front of and behind the load. Duffy’s solutions for finite depth therefore correspond to the solutions we give for line forcing, however in extending to infinite depth he incorrectly argued that the evanescent modes make negligible contribution and thereby omitted the contribution that we find by integrating over the imaginary roots (cf. our Eqn. 37). Also in 1991, Strathdee *et al.*[33] considered a moving point load on floating ice and inverted the spatial Fourier transform numerically. They consider a thick elastic plate for the ice, as well as a thin-plate model and conclude, erroneously, that the thin plate approximation cannot be used close to the load. Their results show singular displacements for even static loads, disagreeing with our results (cf. Sec. 3.2) and the classic Wyman solution. The horizontal displacement given by their thick-plate model is identical to the gradient of our stable thin-plate solution and we conclude that the thick plate model is unnecessary and that some problem in their numerical procedure renders their conclusions virtually useless.

The broader issues of the fluid loading of vibrating surfaces, such as general ratios of plate/fluid densities, were reviewed by Crighton in 1998 [2]. While those issues are outside the scope of our present study, the solutions presented here may be viewed as a refinement and extension of the methods described in that paper.

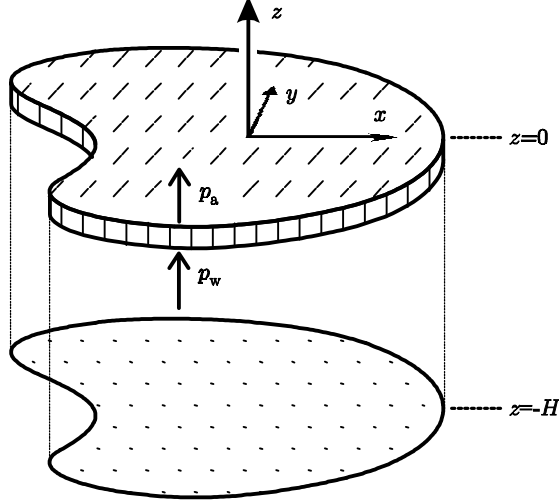


Figure 1: A perspective view of a section of the ice-sheet with the associated water column and sea floor. The coordinate system is shown along with the direction of the applied pressure and the pressure at the ice/water interface.

## 2 The Green's function

### 2.1 Mathematical model

We consider the vertical forcing of a large sheet of floating sea ice, with the forcing occurring at rates at which the ice may be taken to be elastic. The sea ice is modelled as a thin plate floating on water of fixed depth. A section of the ice, water column, and bottom, along with the coordinate system and pressures are depicted in figure 1. Note that the ice is assumed to have negligible thickness and lies at the plane  $\bar{z} = 0$  while the sea bottom is the plane  $\bar{z} = -\bar{H}$ . The  $\bar{x}$ - and  $\bar{y}$ -axes are taken to be in the plane of the ice sheet. The bar over variables is used to denote physical variables, and to distinguish them from the non-dimensional variables that we introduce later. The forcing is via a time-varying applied pressure  $\bar{p}_a$  with restoring force – due to buoyancy and hydrodynamic effects – denoted by  $\bar{p}_w$ .

The resulting mathematical model is given by the system of equations [7, 14]

$$\begin{aligned}
 \bar{p}_i &= L\nabla_{\bar{x},\bar{y}}^4 \bar{\eta} + \bar{m}(\bar{\eta}_{\bar{t}\bar{t}} + g) + \bar{\beta}\bar{\eta}_{\bar{t}} & \bar{z} &= 0 & \text{(thin plate equation)} \\
 \bar{p}_i &= \bar{p}_w + \bar{p}_a & \bar{z} &= 0 & \text{(nett upward pressure)} \\
 \bar{\eta}_{\bar{t}} &= \bar{\phi}_{\bar{z}} & \bar{z} &= 0 & \text{(kinematic condition)} \\
 \rho\bar{\phi}_{\bar{t}} + \bar{p}_w + \rho g\bar{\eta} &= \bar{m}g & \bar{z} &= 0 & \text{(linearized Bernoulli equation)} \\
 \bar{\phi}_{\bar{z}} &= 0 & \bar{z} &= -\bar{H} & \text{(solid bottom)} \\
 \nabla_{\bar{x},\bar{y},\bar{z}}^2 \bar{\phi} &= 0 & -\bar{H} &< \bar{z} < 0 & \text{(in water)}
 \end{aligned} \tag{1}$$

where  $\bar{\eta} = \bar{\eta}(\bar{x}, \bar{y}; \bar{t})$  is vertical displacement of ice from equilibrium,  $\bar{\phi} = \bar{\phi}(\bar{x}, \bar{y}, \bar{z}; \bar{t})$  is velocity potential in the water,  $\rho$  is density of water,  $\bar{m} = \rho_i h$  is the mass density

(per area of surface) of the ice sheet,  $\rho_i$  being the density of ice and  $h$  is thickness of the ice sheet. We have included a positive damping coefficient  $\bar{\beta}$ , to ensure that the model has a unique solution. Solutions are taken in the limit  $\beta \searrow 0$ , and hence we assume that  $\beta$  is infinitesimal.  $L$  is the flexural rigidity of the ice sheet and is usually equated to  $L = Eh^3/12(1-\nu^2)$  when the effective Young's modulus is  $E$ , and Poisson's ratio is  $\nu$ [11]. The nett force acting on the ice is  $\bar{p}_i$  and is positive when acting in the positive  $\bar{z}$ -direction. Note that all pressures and vertical displacements are positive when directed upwards – except, of course, for gravity. We have neglected the constant atmospheric pressure as it does not affect the solution of this dynamic problem; The static weight density of the ice sheet,  $\bar{m}g$ , could have been similarly omitted.

This system of equations may be reduced by using the nett pressure equation and the linearized Bernoulli equation to substitute for  $\bar{p}_i$ , and  $\bar{p}_w$  in the remaining equations. We find that

$$L\nabla_{\bar{x},\bar{y}}^4\bar{\eta} + \bar{m}\bar{\eta}_{\bar{t}\bar{t}} + \bar{\beta}\bar{\eta}_{\bar{t}} + \rho g\bar{\eta} + \rho\bar{\phi}_{\bar{t}} = \bar{p}_a \quad \text{at } \bar{z} = 0 \quad (2)$$

in which the term in the velocity potential must be resolved by solving the partial-differential equation  $\nabla_{\bar{x},\bar{y},\bar{z}}^2\bar{\phi} = 0$  for  $-\bar{H} < \bar{z} < 0$ , along with boundary conditions given by equation 2 and the bottom condition that  $\bar{\phi}_{\bar{z}} = 0$  at  $\bar{z} = -\bar{H}$ .

## 2.2 Non-dimensional formulation

Our nondimensionalization of equation 2 is primarily based on the dispersion equation for deep water. The derivation of, and some properties of, the scaling is discussed later in section 4. The primary scaling, that captures significant physical structure of the problem, is achieved by scaling distance in the plane of the ice sheet by the characteristic length of the ice sheet and scaling time by the characteristic time

$$l_c = \left(\frac{L}{\rho g}\right)^{1/4} \quad \text{and} \quad t_c = \sqrt{\frac{l_c}{g}},$$

respectively. Accordingly, we introduce the non-dimensional coordinates  $x = \bar{x}/l_c$ ,  $y = \bar{y}/l_c$ , and  $t = \bar{t}/t_c$ .

Secondary scaling, which is simply multiplying through each equation to remove dimensional quantities, is achieved by introducing the non-dimensional quantities  $z = \bar{z}/l_c$ ,  $\eta = \bar{\eta}/l_c$ ,  $p_a = \bar{p}_a/\rho g l_c$ ,  $\beta = \bar{\beta}/\rho\sqrt{g l_c}$ ,  $m = \bar{m}/\rho l_c$ ,  $\phi = \bar{\phi}/l_c\sqrt{g l_c}$ ,  $H = \bar{H}/l_c$ . The governing equations then take the non-dimensional form

$$\nabla_{x,y}^4\eta + m\eta_{tt} + \beta\eta_t + \eta + \phi_t = p_a \quad \text{at } z = 0 \quad (3)$$

where the velocity potential is determined by solving Laplace's equation

$$\nabla_{x,y,z}^2\phi = 0 \quad -H < z < 0 \quad (4)$$

with the bottom condition that

$$\phi_z = 0 \quad z = -H \quad (5)$$

and is related to the displacement by the non-dimensional form of the kinematic condition that

$$\phi_z = \eta_t \quad z = 0. \quad (6)$$

Equations 3, 4, 5, and 6 form the system that we will solve for  $\eta$ . The solution we report is for the limit  $\beta \searrow 0$ ; We will not discuss this coefficient much since its role is the standard one of selecting the causal solution [41] which enters our derivation by determining that only outward-going travelling waves are to be included in the solution.

In the deep-water case  $H \approx \infty$ , we will show in subsection 4.3 that the solution is qualitatively unaffected by setting  $m = 0$  for typical values of  $m$  for sea ice. The governing equations then contain no coefficients depending on the physical properties of the ice or water.

### 2.2.1 Point and line forcing

We will solve the system of equations 3, 4, 5, and 6 for two types of surface forcing: where unit force is localized at the origin,  $x = y = 0$ , i.e.,

$$p_a = \delta(x, y) p_a(t), \quad (7)$$

and where unit force per unit length is applied along the line  $y = 0$ , i.e.,

$$p_a = \delta(x) p_a(t) \quad (8)$$

(in both cases  $z = 0$ ). We will denote the resulting surface displacements, for point and line forcing, by  $\eta_P$  and  $\eta_L$ , respectively.

Since the physical properties of the water/ice system, and the system of equations, are invariant under translations and rotations in the plane of the ice sheet, it follows that the surface responses are functions of distance from the applied pressure, only. Further, the response to loading at any point, or along any line, may be found by translating and rotating the solutions we find. Since all other possible (finite energy) forcing, with any given space and time dependence, can be written as a linear combination of such forces and as the system is linear, the resulting motion due to such forces can be found by a superposition of the responses derived here.

## 2.3 Spatial Fourier transform

The solution of equations 3, 4, 5, and 6 is found by taking the 2-dimensional spatial Fourier transform in the plane of the ice sheet for point forcing, and the 1-dimensional spatial Fourier transform in the  $x$ -direction for line forcing. In both cases we solve the resulting equations in the Fourier domain and then inverse transform to spatial variables.

For both point and line forcing, the spatial Fourier transform decomposes the delta-function in equations 7 and 8 into an integral over the wave-like forcing functions

$$p_a(\mathbf{k}) = \exp(i\mathbf{k} \cdot \mathbf{r}). \quad (9)$$

Here  $\mathbf{r} = (x, y)$  and  $\mathbf{k} = (k_x, k_y)$  is the wave number and takes on all possible values in  $\mathbb{R}^2$  for point forcing, and all values of the form  $(k_x, 0)$  for line forcing. Since the system is linear and invariant under shifts in the plane of the ice sheet, the functions  $\phi$  and  $\eta$  will also have  $\exp(i\mathbf{k} \cdot \mathbf{r})$  dependence in the plane of the ice sheet.

We will write the spatial transform of the functions  $\phi$  and  $\eta$  as  $\phi(k_x, k_y, z)$  and  $\eta(k_x, k_y)$ , respectively, and solve for those transform variables. That is, we use the same symbol for the transformed functions, the operation of each function is implicitly defined by the type of arguments it takes.

### 2.3.1 Response to wave-like forcing

For each wave-like forcing component given in equation 9, we solve the system as follows. Since the velocity potential  $\phi$  satisfies Laplace's equation, the Fourier transform with respect to  $x$  and  $y$  satisfies the ordinary differential equation

$$\frac{\partial^2 \phi}{\partial z^2}(k_x, k_y, z) - (k_x^2 + k_y^2) \phi(k_x, k_y, z) = 0$$

which can be solved to determine that  $\phi(k, z) = A(k) e^{kz} + B(k) e^{-kz}$ , i.e.,  $\phi$  is solely a function of the magnitude of the wave-number  $k = \|\mathbf{k}\|$ . The boundary condition that  $\phi_z|_{z=-H} = 0$  further restricts the coefficients to  $A(k) = C e^{kH}$ , and  $B(k) = C e^{-kH}$ . Thus the depth-dependence of the potential due to wave-like forcing is

$$\phi(k, z) = \phi(k, 0) \frac{\cosh k(z + H)}{\cosh kH}. \quad (10)$$

At the surface,  $z = 0$ , the vertical component of the velocity is  $\phi_z(k, 0) = \phi(k, 0) k \tanh kH$ . Using this relationship to substitute for  $\phi_z$  in the non-dimensional form of the kinematic condition, we find that

$$\phi = \frac{\eta_t}{k \tanh kH} \quad \text{at } z = 0 \quad (11)$$

and hence, differentiating with respect to normalized time,  $\phi_t = \eta_{tt}/k \tanh kH$  at  $z = 0$ . Substituting for  $\phi_t$  in equation 3 we get the single ordinary differential equation for each spatial Fourier component of  $\eta$

$$\left( m + \frac{1}{k \tanh kH} \right) \eta_{tt} + \beta \eta_t + (1 + k^4) \eta = p_a. \quad (12)$$

As mentioned earlier, Sneddon's solution method [27], also used in subsequent work [24, 25, 29], is to write the solution of this equation with initial conditions as the (temporal) convolution of the right-hand side with the causal fundamental solution, leaving that calculation and the required inverse (spatial) Fourier transform to be performed for specific loadings  $p_a(x, y, t)$ . In contrast, we focus on forcing with harmonic time dependence and actually perform the inverse Fourier transform.

## 2.4 Harmonic forcing

We now restrict our attention to forcing that is harmonic in time, i.e., with time dependence  $\exp(i\omega t)$ , where  $\omega$  is the non-dimensional radial frequency corresponding to the physical period of forcing  $\bar{T} = 2\pi t_c/\omega$ .

As the system of equations is also linear and invariant in time, it follows that the surface displacement  $\eta$  and the velocity potential  $\phi$  have the same harmonic time dependence as the forcing. In particular,  $\eta(x, y, t) = \eta(r) \exp(i\omega t)$ , and similarly for  $\phi$ , where  $r$  is the distance from the forcing which equals  $\sqrt{x^2 + y^2}$  for point forcing and  $|x|$  for line forcing. We will omit writing the  $\exp(i\omega t)$  time dependence from now on, and take it to be implicit.

### 2.4.1 Dispersion equation

Using the equivalence  $\partial/\partial t \equiv i\omega$ , we find that (the spatial Fourier transform of) the displacement of the ice sheet for both types of forcing is

$$\eta(k) = \frac{1}{d(k, \omega)} \quad (13)$$

where

$$d(k, \omega) = k^4 + 1 - m\omega^2 + i\beta\omega - \frac{\omega^2}{k \tanh kH} \quad (14)$$

is the dispersion equation for waves propagating through an ice sheet. We have set  $p_a = 1$  as that is the coefficient of  $\exp(i\mathbf{k} \cdot \mathbf{r})$  in the forcing. Note that  $\eta$  is a function of the *magnitude* of the wave number only, which is not surprising as the geometry is circularly symmetric with no preferred direction of propagation.

The roots of the dispersion equation, for fixed  $\omega$ , are the poles of the function  $\eta(k)$ . Later, we will use the observation that the dispersion equation  $d(k, \omega)$  is an even function of  $k$ , and hence if  $k_0$  is a root then so is  $-k_0$ . For fixed  $\omega \neq 0$  and for  $\beta = 0$ , it is known[39] that equation 14 has two real roots  $\pm k_T$  ( $k_T > 0$ ) corresponding to travelling waves, four complex roots occurring as plus and minus a complex-conjugate pair  $\pm k_D$  and  $\pm k_D^*$  ( $\text{Re}(k_D) > 0$  and  $\text{Im}(k_D) > 0$ ) corresponding to damped-travelling waves, and a countably infinite set of imaginary roots  $\{\pm ik_n\}_{n=1,2,\dots}$ , ( $k_n > 0$ ) where, for typical cases  $m\omega^2 \leq 1$ ,  $(n - \frac{1}{2})\pi < k_n H < n\pi$  each corresponding to an evanescent mode.

We may also solve for the velocity potential at the surface of the water

$$\phi(k, 0) = \frac{i\omega\eta}{k \tanh kH} = \frac{i\omega}{k \tanh(kH) d(k, \omega)} \quad (15)$$

which is also a function of  $k$  only and has the same poles as  $\eta(k)$ .

## 2.5 Inverse Fourier transform

The surface displacement for point forcing is given by the 2-dimensional inverse Fourier transform of  $\eta(k)$  in equation 13 and, since  $\eta(k)$  is radially symmetric, the

inverse transform may be written [31]

$$\eta_{\text{P}}(r) = \frac{1}{2\pi} \int_0^{\infty} \eta(k) k J_0(kr) dk \quad (16)$$

where  $r$  is the distance from the point of forcing. The response to line forcing is given by the inverse Fourier transform of  $\eta(k)$  in the  $x$ -direction and, since  $\eta(k)$  is an even function, this is

$$\eta_{\text{L}}(r) = \frac{1}{\pi} \int_0^{\infty} \eta(k) \cos(kr) dk \quad (17)$$

where again  $r$  is the distance from the line of forcing. The factors  $1/2\pi$  and  $1/\pi$  result from the definition of the forward transform that we assumed.

Let  $K^{\wedge}$  denote the set of roots of the dispersion equation with positive imaginary part when  $\beta > 0$ . This set is  $K^{\wedge} = \{k_{\text{T}}, k_{\text{D}}, -k_{\text{D}}^*, ik_1, ik_2, ik_3, \dots\}$ . Note that the remaining roots are the negative of the values in  $K^{\wedge}$ . Since  $\eta(k)$  is an even fractional function that equals zero when  $k = 0$  and is bounded in the whole plane except in regions around its poles,  $\eta(k)$  can be expressed using the Mittag-Leffler expansion which, after pairing each pole  $q \in K^{\wedge}$  with  $-q$ , gives ([9] appendix B)

$$\eta(k) = \sum_{q \in K^{\wedge}} \frac{2qR(q)}{k^2 - q^2}$$

where  $R(q)$  is the residue of  $\eta$  at  $q$ . By substituting this expansion into the integrals in equations 16 and 17, we are able to perform the integration and write each result as a summation.

Using the identities ([35] formula 11.4.44 with  $\nu = 0$ ,  $\mu = 0$ ,  $z = -iq$  and  $a = r$ )

$$\int_0^{\infty} \frac{k}{k^2 - q^2} J_0(kr) dk = K_0(-iqr) \quad \text{for } \text{Im } q > 0, r > 0$$

and ([35] formula 9.6.4)  $K_0(z) = \frac{\pi i}{2} H_0^{(1)}(iz)$ , holding for  $\text{Re } z \geq 0$ , the displacement for point forcing may be written in the alternative forms

$$\eta_{\text{P}}(r) = \frac{1}{\pi} \sum_{q \in K^{\wedge}} qR(q) K_0(-iqr) \quad (18)$$

$$= \frac{i}{2} \sum_{q \in K^{\wedge}} qR(q) H_0^{(1)}(qr). \quad (19)$$

The identity ([38] formula 1.2 (11) with  $x = k$ ,  $y = r$ , and  $a = -iq$ )

$$\int_0^{\infty} \frac{\cos(kr)}{k^2 - q^2} dk = -\frac{\pi}{2iq} \exp(iqr) \quad \text{for } \text{Im } q > 0, r > 0$$

gives the surface displacement for line forcing

$$\eta_{\text{L}}(r) = i \sum_{q \in K^{\wedge}} R(q) \exp(iqr). \quad (20)$$

### 2.5.1 Residues of $\eta(k)$

Since each of the poles of  $\eta(k)$  is simple, the residue  $R(q)$  at a pole  $q$  can be found using the expression

$$\begin{aligned} R(q) &= \left( \frac{d}{dk} d(k, \omega) \Big|_{k=q} \right)^{-1} \\ &= \left( 4q^3 + \omega^2 \left( \frac{qH + \tanh qH - qH \tanh^2 qH}{q^2 \tanh^2 qH} \right) \right)^{-1}. \end{aligned} \quad (21)$$

As each pole  $q$  is a root of the dispersion equation, we may substitute  $\tanh qH = \omega^2 / (q^5 + uq)$ , where for brevity we have defined  $u = (1 - m\omega^2)$ . Taking the limit  $\beta \searrow 0$ , the residue may then be given as the rational function of the pole

$$R(q) = \frac{\omega^2 q}{\omega^2 (5q^4 + u) + H ((q^5 + uq)^2 - \omega^4)}. \quad (22)$$

This form avoids calculation of the hyperbolic tangent which becomes small at the imaginary roots causing numerical round-off problems.

While the expressions in equations 21 and 22 coincide when the argument is one of the poles, note that the two functions do not coincide for all arguments. The expression in equation 21 is a rapidly varying function near each pole whereas, in contrast, the expression in equation 22 is a smooth function of its argument. This latter property is important and we will exploit it to find a simple expression for the surface displacement when the water is deep.

We denote the residues for the poles in  $K^\wedge$  by  $R_T = R(k_T)$ ,  $R_D = R(k_D)$ , and  $R_n = R(ik_n)$ ,  $n \in \mathbb{N}$ , respectively. Note that  $R(-k_D^*) \rightarrow -R_D^*$  as  $\beta \rightarrow 0$ .

## 2.6 Summary of calculating the Green's function

The Green's function for finite water depth  $H$  is found by first finding the roots in the upper-half plane  $K^\wedge = \{k_T, k_D, -k_D^*, ik_1, ik_2, ik_3, \dots\}$  of the dispersion equation 14, truncated after some finite number of roots. Straight forward computer code (in MatLab) to find the roots has been given by Fox [9]. After calculating the residue for each root as in equation 22 one then computes the sum

$$\begin{aligned} \eta_P(r) &= \frac{i}{2} \sum_{q \in K^\wedge} q R(q) H_0^{(1)}(qr) \\ &= \frac{i}{2} k_T R_T H_0^{(1)}(k_T r) - \text{Im} \left[ k_D R_D H_0^{(1)}(k_D r) \right] + \frac{1}{\pi} \sum_{n=1}^{\infty} ik_n R_n K_0(k_n r) \end{aligned} \quad (23)$$

to find the surface displacement resulting from point forcing. The step to the last line uses the identities  $-i(-k_D^*) = (-ik_D)^*$  and  $H_0^{(1)}(-z^*) = -\left(H_0^{(1)}(z)\right)^*$ . Since  $|qR(q)| \propto |q|^{-8}$  as  $|q|$  increases, hence the sum may be terminated after a relatively small number of terms without significant error. The physical displacement when

$\bar{p}_a = \delta(\bar{x}) \delta(\bar{y}) \exp\{i\bar{\omega}\bar{t}\}$  is found by scaling the non-dimensional solution according to

$$\bar{\eta}_P(\bar{x}, \bar{y}) = \frac{1}{\rho g l_c^2} \eta_P(\bar{r}/l_c) \quad (25)$$

where  $\bar{r} = \sqrt{\bar{x}^2 + \bar{y}^2}$ .

The surface displacement for line forcing is given by the sum

$$\eta_L(r) = i \sum_{q \in K^+} R(q) \exp(iqr) \quad (26)$$

$$= iR_T \exp(ik_T r) - 2 \operatorname{Im} [R_D \exp(ik_D r)] + i \sum_{n=1}^{\infty} R_n \exp(-k_n r). \quad (27)$$

The physical displacement for the line forcing  $\bar{p}_a = \delta(\bar{x}) \exp\{i\bar{\omega}\bar{t}\}$  is found by scaling this non-dimensional solution as

$$\bar{\eta}_L(\bar{x}, \bar{y}) = \frac{1}{\rho g l_c} \eta_P(|\bar{x}|/l_c). \quad (28)$$

Since  $iR_n$  is real for each  $n = 1, 2, \dots, \infty$ , we see that the contribution due to the evanescent modes in equations 24 and 27 is always real. Hence the only imaginary term in the responses due to point or line loading is the coefficient of the travelling wave, corresponding to the travelling waves being the only modes that carry energy away from the load. The damped-travelling and evanescent modes contribute motion that is in phase with the forcing while the travelling mode has a component in quadrature to the forcing.

The potential throughout the water can be found by evaluating a similar inverse Fourier transform. The resulting potential in cylindrical coordinates for point forcing is

$$\phi_P(r, z) = -\frac{\omega}{2} \sum_{q \in K^+} \frac{R(q)}{\sinh qH} H_0^{(1)}(qr) \cosh q(z + H)$$

and for line forcing is

$$\phi_L(r, z) = -\omega \sum_{q \in K^+} \frac{R(q)}{q \sinh qH} \exp(iqr) \cosh q(z + H).$$

The term  $\sinh qH$  is close to zero for most imaginary roots so these expressions are not directly suitable for computation. The substitution following equation 21 may be used to give computationally stable expressions.

## 2.7 Description of modes

Each of the roots of the dispersion equation,  $q \in K^+$ , gives the wavenumber of a *natural mode* of the floating ice sheet. So the surface displacement, given in equations 23 and 26, are representations of the solution as a sum over these natural modes. It is instructive to examine the form of each mode.

The modes for line forcing are of the form  $\exp(iq|x|)$  which are planar waves, while the modes generated by point forcing are of the form  $H_0^{(1)}(qr)$  which are cylindrically-spreading waves. In both cases, the positive real root (when  $\beta = 0$ ) gives rise to a wave that propagates energy into the far field. For line forcing this travelling wave has constant amplitude with distance while the cylindrical spreading that occurs with point forcing gives the wave an amplitude proportional to  $1/\sqrt{r}$  in the far field. The complex roots give damped-travelling waves that oscillate with an amplitude that decays, or grows, away from the location of forcing with the decay being exponential for line forcing and more rapidly for point forcing. The roots that are pure imaginary, when  $\beta = 0$ , give evanescent modes that have no propagating component and decay, or grow, rapidly away from the point of forcing. The evanescent modes are simply exponentials for line forcing and modified Bessel functions in the case of point forcing.

Because of their unbounded growth, the damped-travelling and evanescent modes can only exist in the region near the forcing or, more generally, at boundaries of regions over which the constant-coefficient homogeneous equation applies, i.e. at transitions in  $p_a$  or transitions in the mechanical properties. When that boundary is infinite in extent (such as our line of forcing), these modes are sometimes referred to as edge- or boundary-waves [20]. Each of the damped-travelling and evanescent modes also have the property of containing non-zero energy but with no net energy propagation away from the inhomogeneity. For this reason they are sometimes referred to as trapped waves [21]. In our case, the system only has such a transition at the point or line of forcing and these modes have significant value near the forcing only, with each mode decaying rapidly away from the forcing.

As an aside we note that from the perspective of those who study the Laplacian operator, all the modes we have described are evanescent modes of the Laplacian. However, the nomenclature we use is useful when discussing the form of the wave that propagates at the surface of the water.

### 3 Response in special cases

While the infinite sums in equations 23 and 26 give the exact surface displacement for  $r > 0$ , other forms are more convenient for some computational purposes. In this section we develop simplified expressions for the response in limiting geometries which are of typical interest. In section 3.1 we examine the case where the water is deep, and in section 3.2 we derive expressions for the deflection at the location of the applied force. In sections 3.3 and 3.4 we give simplified expressions for the response in the near field and far field, respectively.

#### 3.1 Deflection for deep water

The solutions take particularly simple forms when the water is very deep, i.e. in the limit  $H \rightarrow \infty$ . As  $H \rightarrow \infty$ , the imaginary roots of the dispersion equation approach  $i$  times the zeros of  $\tan(kH)$  and hence are evenly spaced with spacing  $i\pi/H$ . In the limit these roots form a continuum with equal density over the imaginary axis. The sum over these roots may then be calculated as an integral over the positive

imaginary semi-axis. For both types of forcing, the solutions are then given by a sum over special functions at wavenumbers given by the roots of a fifth-order polynomial.

The residue at a root of the dispersion equation in equation 22 tends to

$$R(q) \rightarrow \frac{1}{H}Q(q) \quad \text{as } H \rightarrow \infty \quad (29)$$

where

$$Q(q) = \frac{\omega^2 q}{(q^5 + uq)^2 - \omega^4}. \quad (30)$$

The sum over the imaginary roots in the response to point loading in equation 24 is then

$$\begin{aligned} \frac{1}{\pi} \sum_{n=1}^{\infty} ik_n R_n K_0(k_n r) &\rightarrow \frac{1}{\pi} \sum_{n=1}^{\infty} \frac{in\pi}{H} Q\left(\frac{in\pi}{H}\right) K_0\left(\frac{n\pi}{H}r\right) \\ &\rightarrow \frac{1}{\pi^2} \int_0^{\infty} ikQ(ik) K_0(kr) dk. \end{aligned} \quad (31)$$

Similarly, the sum over imaginary roots for line loading in equation 27 is

$$i \sum_{n=1}^{\infty} R_n \exp(-k_n r) \rightarrow \frac{1}{\pi} \int_0^{\infty} iQ(ik) \exp(-kr) dk. \quad (32)$$

The integrals in equations 31 and 32 can be evaluated by first writing  $Q$  as a sum over simple poles as we did for the inverse Fourier transform. Classification of the poles of  $Q$  is conveniently achieved by first noting that  $Q(q) = (v(q) - v(-q))/2$  where

$$v(q) = \frac{q}{q^5 + uq - \omega^2}. \quad (33)$$

When  $\omega \neq 0$ ,  $v(q)$  and  $v(-q)$  have no poles in common and hence poles of  $v$  are also poles of  $Q$ . It follows that all poles of  $Q$  are plus and minus the poles of  $v$ . Since  $v$  and  $\eta$  (in the limit  $H \rightarrow \infty$ ) coincide for arguments with positive real part, the poles of  $\eta$  with positive real part, i.e.  $k_T, k_D$ , and  $k_D^*$ , are also roots of  $v$  and hence  $Q$ . There are two further roots of  $v$  with negative real part, which we denote  $k_E$  and  $k_E^*$ , with  $k_E$  chosen to have positive imaginary part. It can be shown that  $\text{Im}(k_E) > 0$  for any finite mass density  $m$ , and hence  $k_E$  is never real.

Let  $K_v = \{k_T, k_D, k_D^*, k_E, k_E^*\}$  denote the set of poles of  $v$ . The residue of  $v$  at a pole  $q \in K_v$  is

$$R_v(q) = \frac{q^2}{5\omega^2 - 4uq}. \quad (34)$$

Note that the residues at  $k_T, k_D$  and  $k_D^*$ , are the same as defined in equation 22 and we denote these  $R_T, R_D$  and  $R_D^*$ , as before, respectively. Write  $R_E = R_v(k_E)$  and hence  $R_E^* = R_v(k_E^*)$ . The residues of  $Q$  are 1/2 the residue of  $v$ .

The integral in equation 31 may be evaluated using the partial-fraction expansion

$$ikQ(ik) = - \sum_{q \in K_v} \frac{q^2 R_v(q)}{k^2 + q^2} \quad (35)$$

and the integral ([35] formula 11.4.47 with  $\nu = 0$ ,  $t = k$ ,  $r = a$ ),

$$\int_0^\infty \frac{K_0(kr)}{(k^2 + q^2)} dk = \frac{\pi^2}{4q} [\mathbf{H}_0(qr) - Y_0(qr)],$$

holding for  $\text{Re } q > 0$  since we always take  $r > 0$ . Here  $\mathbf{H}_0$  is a Struve function of zero order. It is convenient for notational brevity, as well as computational efficiency, to use the function  $h(rz) = \mathbf{H}_0(rz) - Y_0(rz)$ . Performing the integral in equation 31 and combining conjugate-pair poles, equation 24 for the response to point forcing in the deep water limit can be written in terms of poles of  $v$  as,

$$\begin{aligned} \eta_P(r) = & \frac{i}{2} k_T R_T H_0^{(1)}(k_T r) - \text{Im} \left[ k_D R_D H_0^{(1)}(k_D r) \right] \\ & - \frac{k_T R_T}{4} h(k_T r) - \frac{1}{2} \text{Re}(k_D R_D h(k_D r)) + \frac{1}{2} \text{Re}(k_E R_E h(-k_E r)). \end{aligned} \quad (36)$$

The pole  $-k_E$  of  $Q$  has been used since  $\text{Re}(-k_E) > 0$ . Note that only the first, travelling wave, term is imaginary which corresponds to that mode being the only one that propagates energy away from the point of forcing. The remaining terms give displacements that are in phase with the forcing.

The integral in equation 32 for line loading may be found using the expansion

$$iQ(ik) = \sum_{q \in K_v} \frac{k R_v(q)}{k^2 + q^2}$$

and the integral ([35] formula 5.2.13 with  $t = k/q$  and hence  $z = qr$  and formula 5.2.7)

$$\int_0^\infty \frac{k \exp(-kr)}{k^2 + q^2} dk = -\text{Ci}(qr) \cos(qr) - \text{si}(qr) \sin(qr)$$

holding for  $\text{Re}(q) > 0$  since  $r$  is positive real. Here Ci and si are cosine integral and sine integral functions, respectively. As with the point-forcing case, notation and computation are simplified by defining the function  $g(qr) = -\text{Ci}(qr) \cos(qr) - \text{si}(qr) \sin(qr)$ . Combining conjugate-pair poles, equation 27 for the response to line forcing in the deep water limit can be written as,

$$\begin{aligned} \eta_L(r) = & i R_T \exp(ik_T r) - 2 \text{Im} [R_D \exp(ik_D r)] \\ & + \frac{R_T}{\pi} g(k_T r) + \frac{2}{\pi} \text{Re} [R_D g(k_D r)] + \frac{2}{\pi} \text{Re} [R_E g(-k_E r)]. \end{aligned} \quad (37)$$

where, again, the pole  $-k_E$  has been used.

### 3.2 Deflection at the location of forcing

The expressions for the surface displacement at the position of point forcing given so far, based on equations 18 or 19, may not be used to calculate the surface displacement at the position of point forcing because of the log-like singularity in the Bessel functions as  $r \rightarrow 0$ . Some authors [33] have erroneously concluded that use of the thin-plate model for the ice sheet leads to predicting a singularity in displacement at the point of forcing. We now establish that the coefficient of the singular terms is, in fact, zero and the surface displacement is finite, and smooth, at the point of forcing.

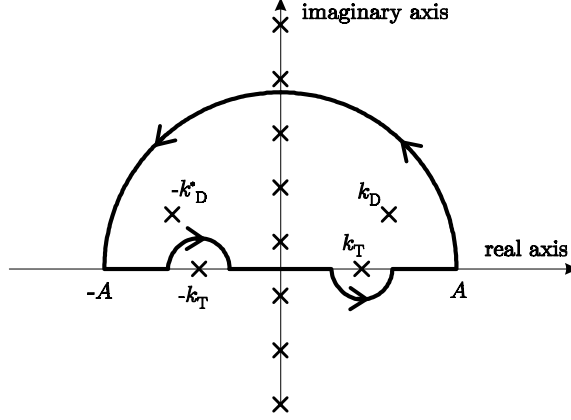


Figure 2: Contour used for integration with approximate pole positions shown as crosses.

### 3.2.1 Deflection at the point of forcing

Strictly, expression 23 does not hold at the point of forcing  $r = 0$  as it requires the sum of terms that are singular. However, since the plate equation is fourth order and Lapace's equation is second order, we would expect the solution to be smooth everywhere, including when  $r = 0$ . We now derive a summable expression for the displacement at the point of forcing.

The modified Bessel function  $K_0(z)$  has the polynomial form

$$K_0(z) = -\log\left(\frac{z}{2}\right) I_0(z) + \sum_{l=0}^{\infty} \frac{(z/2)^{2l}}{(l!)^2} \psi(l+1),$$

where  $I_0$  and  $\psi$  are the modified Bessel function and the Psi function, respectively ([35] formulas 9.6.12 and 9.6.13). When  $|z|$  is small,  $K_0(z) \approx -\log z + c$  in which the constant  $c = \log 2 - \gamma$ . Hence, as  $r \rightarrow 0$ , the infinite series in 18 approaches

$$\begin{aligned} \eta_P(r) &\rightarrow \frac{1}{\pi} \sum_{q \in K^+} qR(q) (-\log(-iqr) + c) \\ &= -\frac{1}{\pi} \sum_{q \in K^+} qR(q) \log(-iq) + \frac{c - \log r}{\pi} \sum_{q \in K^+} qR(q) \end{aligned} \quad (38)$$

Consider now a contour integration of the function  $\eta(k)k$ , anti-clockwise along the contour shown in Figure 2. The arc of radius  $A$  is chosen to avoid the poles on the imaginary axis, and the arcs around the poles on the real-axis are taken to have small radius. Since  $\eta(k)k$  is an odd function, the integral over the real axis, including the two small arcs, is zero. Further, as  $A \rightarrow \infty$ ,  $\eta(k)k$  tends to zero faster than  $A^{-2}$  on the semi-circle of radius  $A$ , the integral over the semi-circle tends to zero as  $A \rightarrow \infty$ . Hence the integral over the whole contour tends to zero as  $A \rightarrow \infty$ . Since this limit equals a constant multiplied by the sum of the residues of  $\eta(k)k$  at the poles enclosed

within the contour, the sum of residues of  $\eta(k)k$  at poles in the upper half plane is zero, i.e.,

$$\sum_{q \in K^+} qR(q) = 0.$$

We immediately see that the term multiplied by  $(c - \log r)/\pi$  in equation 38 is zero. Thus at  $r = 0$  the complex displacement takes the value

$$\eta_P(0) = -\frac{1}{\pi} \sum_{q \in K^+} qR(q) \log(-iq) = -\frac{1}{\pi} \sum_{q \in K^+} qR(q) \log(q). \quad (39)$$

Since  $qR(q)$  decreases as  $k_n^{-8} \propto n^{-8}$  for the evanescent modes, relatively few terms are required to evaluate this sum accurately.

Figure 3 shows the displacement at the point of forcing as a function of frequency and for water depths  $H = 20\pi$ ,  $2\pi$ , and  $0.2\pi$ . The depths are taken as multiples of  $2\pi$  since that is the wavelength of the travelling wave with unit non-dimensional wavenumber. Water depths greater than  $20\pi$  give visually identical deflections, so the

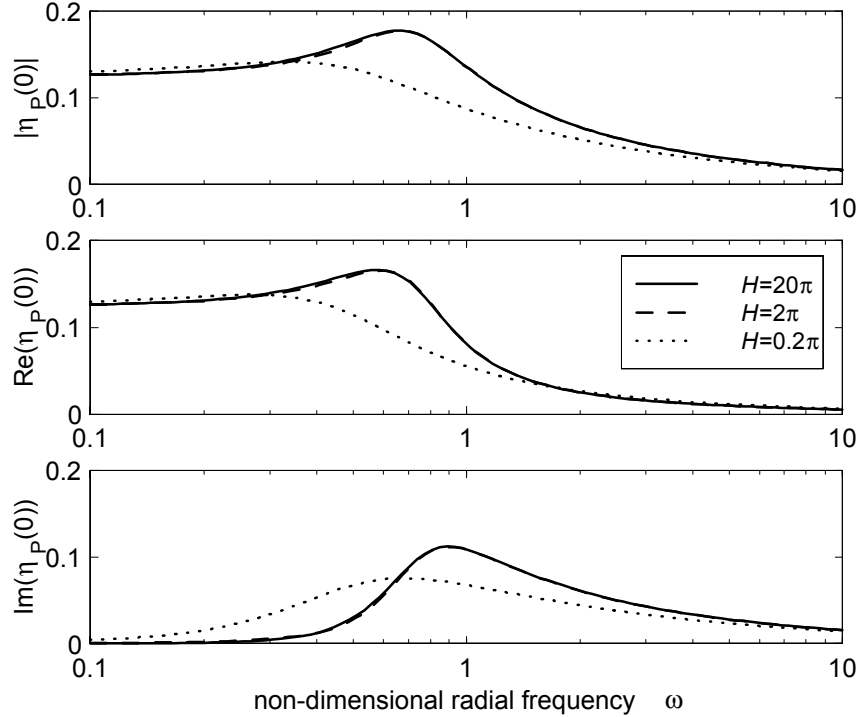


Figure 3: Top to bottom shows the magnitude, real part and imaginary part of the complex displacement at the point of forcing as a function of non-dimensional frequency. The non-dimensional water depths  $H = 2\pi \times 10$ ,  $2\pi \times 1$ ,  $2\pi \times 0.1$ , are shown. In all cases we take  $m = 0$ .

curve for  $H = 20\pi$  may be taken as the deep-water solution. Note that the solution for  $H = 2\pi$  is nearly identical to the deep-water solution at all frequencies, and hence  $H = 2\pi$  may be considered “deep” for point forcing.

The imaginary part of the response is proportional to the average power that the load puts into the ice. Equation 39 can be rewritten as

$$\eta_{\text{P}}(0) = -\frac{1}{\pi} \left( k_{\text{T}} R_{\text{T}} \log(k_{\text{T}}) + 2 \operatorname{Re} [k_{\text{D}} R_{\text{D}} \log(-ik_{\text{D}})] + \sum_{n=1}^{\infty} ik_n R_n \log(k_n) \right) + i \frac{k_{\text{T}} R_{\text{T}}}{2}$$

and, since  $ik_n R_n$  is real, we see that the imaginary part is just the coefficient of the travelling mode. This corresponds to the travelling mode being the only mode that carries energy away from the point of forcing.

### 3.2.2 Deflection on the line of forcing

Because the exponentials in equation 26 are regular at  $r = 0$ , the displacement at the line of forcing may be found by setting  $r = 0$  directly to give

$$\eta_{\text{L}}(0) = \sum_{q \in K^+} iR(q). \quad (40)$$

Using this expression, the absolute value, real and imaginary part of the complex deflection, as a function of frequency, are shown in figure 4 for water depths of  $H = 20\pi$ ,  $2\pi$ , and  $0.2\pi$ . Water depths of  $20\pi$  and greater give visually identical deflections, so the curve for  $H = 20\pi$  may be taken as the deep-water solution.

As for the point-loading case, only the travelling mode contributes to the imaginary part of equation 40, and hence the graph of the imaginary part of the displacement is essentially a plot of the amplitude of the travelling wave generated and also the energy generated by the forcing.

Note that the displacements for the water depths  $H = 20\pi$  and  $H = 2\pi$  differ for frequencies below 1. Hence the load on the forcing mechanism and the resulting displacements are affected by water depth when  $H \approx 2\pi$  and this depth cannot be considered to be “deep”. This is in contrast to the point loading case where  $H = 2\pi$  is effectively deep.

### 3.2.3 Deep water

The displacement at the point of forcing when the ice is floating on deep water may be found by evaluating the finite-depth solution in equation 39 in the limit  $H \rightarrow \infty$ . The sum over evanescent modes is

$$-\frac{1}{\pi} \sum_{n=1}^{\infty} ik_n R(ik_n) \log(k_n) \rightarrow -\frac{1}{\pi^2} \int_0^{\infty} ikQ(ik) \log(k) dk.$$

Using the expansion in equation 35 and the integral ([38] section 14.2 (24) with  $a = -iq$ , and  $y = iq$ )

$$\int_0^{\infty} \frac{\log x}{x^2 + q^2} dx = \frac{\pi}{2q} \log q \quad \operatorname{Re} q > 0$$

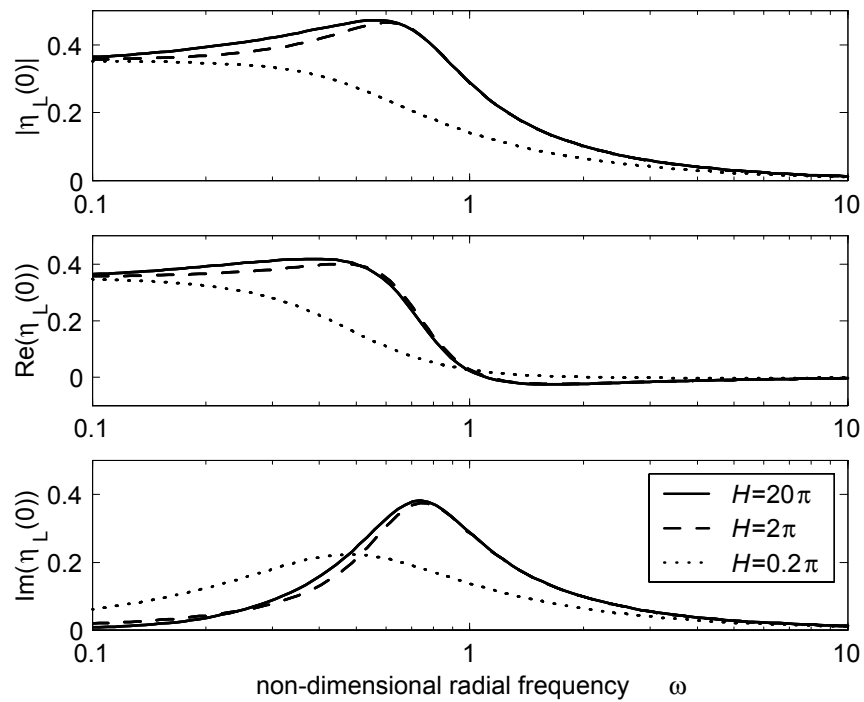


Figure 4: Top to bottom shows the magnitude, real part, and imaginary part of the complex displacement on the line of forcing as a function of non-dimensional frequency for the non-dimensional water depths  $H = 2\pi \times 10$ ,  $2\pi \times 1$ ,  $2\pi \times 0.1$ . We take  $m = 0$ .

we find that

$$\eta_P(0) = i\frac{k_T R_T}{2} - \frac{k_T R_T}{2\pi} \log(k_T) - \frac{1}{\pi} \operatorname{Re}(k_D R_D \log(-k_D)) - \frac{1}{\pi} \operatorname{Re}(k_E R_E \log(-k_E)). \quad (41)$$

This gives a very simple expression for finding the displacement at the point of forcing when the water is deep. Hence, equation 41 gives an efficient route to the result computed numerically by Nevel [13]. The imaginary part,  $ik_T R_T/2$ , is maximized when  $\omega = 0.90$ , so that is the frequency of maximum coupling.

Because the cosine integral has a log-like singularity at the origin, equation 37 is not directly suitable for computing the displacement on the line of forcing in the deep-water limit. However, expanding  $\operatorname{ci}(qr)$  in terms of the log plus power series and using the identity  $\sum_{q \in K_v} R_v(q) = 0$  allows us to write

$$\eta_L(0) = iR_T - \frac{R_T}{\pi} \log(k_T) - \frac{2}{\pi} \operatorname{Re}[R_D \log(-k_D)] - \frac{2}{\pi} \operatorname{Re}[R_E \log(-k_E)] \quad (42)$$

which is easily evaluated to give the displacement on the line of forcing when the water is deep. The imaginary part,  $iR_T$ , and hence coupling between the line load and the ice sheet, is maximized when  $\omega = 0.74$ .

### 3.3 Deflection and strain near to point forcing

Consider again the expansion of the Bessel function  $K_0$  in section 3.2.1 within the sum 18, and with a power series expansion of  $I_0$  ([35] formula 9.6.10 with  $\nu = 0$ ). The log and constant terms were dealt with in section 3.2.1 giving  $\eta_P(0)$ . Adding the remaining terms in the power series gives the expression,

$$\eta_P(r) = \eta_P(0) + \frac{1}{\pi} \sum_{q \in K^-} qR(q) \left( \sum_{l=1}^{\infty} \frac{(-q^2 r^2)^l}{4^l (l!)^2} \left( \psi(l+1) - \log\left(\frac{-iqr}{2}\right) \right) \right) \quad (43)$$

for all  $r$ . Though not particularly efficient, equation 43 allows stable calculation of displacement for a range of small  $r$ , i.e., near the point of forcing.

Note that the terms with  $l \geq 1$  have the  $r$ -dependence  $(\log(qr) + c)r^{2l}$  for some constant  $c$  which depends on  $l$ . Since

$$\frac{d}{dr} ((\log(qr) + c)r^{2l}) = r^{2l-1} (1 + 2l(\log(qr) + c))$$

these terms have zero derivative at  $r = 0$ . Hence  $\eta'_P(0) = 0$  as expected. It follows that the displacement function obtained by the method above is regular everywhere.

Often measurements of flexural-gravity waves in ice sheets are measured via the resulting strain at the upper surface. Assuming that the ice sheet may be treated as a uniform thin plate, the surface strain resulting from small point or line loading is proportional to the second derivative of vertical displacement pointing in the  $r$

direction. The second derivative for each term in equation 43 with  $l \geq 1$  has the  $r$ -dependence

$$\frac{d^2}{dr^2} ((\log(qr) + c)r^{2l}) = r^{2l-2} (\log(qr)(4l^2 - 2l) + 4l^2c + 4l - 2lc - 1)$$

which is non-zero at  $r = 0$  only for the  $l = 1$  term. Since  $\sum_{q \in K^*} R(q)q^3 = 1$ , the second derivative of the  $l = 1$  term in equation 43 can be written

$$\frac{d^2}{dr^2} \eta_P(r) \approx \frac{1}{4\pi} \left( 2 \log\left(\frac{r}{2}\right) + 3 - \psi(2) + \sum_{q \in K^*} q^3 R(q) \log(-iq) \right)$$

for small  $r$ . So we see that the strain has a singularity at the origin that behaves like  $\log r$  and is in phase with the forcing.

### 3.4 Far-field deflection

When  $|z|$  is large then ([35] formula 9.2.3)  $H_0^{(1)}(z) \sim \sqrt{\frac{2}{\pi z}} \exp\{i(z - \pi/4)\}$ . Thus, selecting just the term due to the travelling mode in equation 23, the complex displacement far from the point of forcing is

$$\eta_P(r) \sim \frac{\sqrt{k_T} R_T \exp\{i(k_T r + \pi/4)\}}{\sqrt{2\pi} \sqrt{r}} \quad (44)$$

for large  $r$ .

Taking just the travelling-wave component in the deflection for line forcing we find that the deflection far from a line load is

$$\eta_L(x, y) \sim R_T \exp\{i(k_T |x| + \pi/2)\} \quad (45)$$

### 3.5 Static forcing

The deflection due to static loading can be found by setting  $\omega = 0$  in equation 14 to give

$$\eta(k) = \frac{1}{k^4 + 1}$$

and proceeding as we have done for non-zero frequency. Now  $\eta(k)$  has four complex poles,  $\pm e^{i\pi/4}$ ,  $\pm e^{i3\pi/4}$ ; the set of poles in the upper half plane being  $K^* = \{e^{i\pi/4}, e^{i3\pi/4}\}$ . The residue of  $\eta(k)$  at a pole  $q$  is

$$R(q) = \frac{1}{(k^4 + 1)' \Big|_{k=q}} = \frac{1}{4q^3}.$$

The sum in equation 18, scaled as equation 25, gives the physical response to static point force

$$\bar{\eta}_P(\bar{r}) = \frac{\text{kei}(\bar{r}/l_c)}{2\pi \rho g l_c^2} \quad (46)$$

where  $\text{kei}(x)$  is the Kelvin function (of zero order) and we have used the identity ([35] formulas 9.9.2 and 9.6.32)  $2i\text{kei}(x) = K_0(e^{i\pi/4}x) - K_0(e^{-i\pi/4}x)$ . The expression in Eqn. 46 is the same as given by Wyman [36] and the equivalent expression derived earlier by Hertz [15].

The sum in equation 20, scaled as equation 28, gives the physical response to a static line force as

$$\bar{\eta}_L(\bar{x}, \bar{y}) = \frac{1}{2\rho g l_c} \exp\left(\frac{-|\bar{x}|}{\sqrt{2}l_c}\right) \cos\left(\frac{|\bar{x}|}{\sqrt{2}l_c} - \frac{\pi}{4}\right).$$

## 4 Properties of the non-dimensionalization

Our non-dimensionalization is based on the structure of the deep-water dispersion equation for the travelling and damped-travelling waves, i.e., for wavenumbers with positive real part. Note that the deflections given in equations 23 and 26, or 36 and 37, are continuous functions of the roots of the dispersion equation and so simplifying the structure of the roots leads to simplification in the solutions.

For (dimensioned) wavenumbers  $\bar{k}$  with  $\text{Re}(\bar{k}) > 0$ , the deep-water dispersion equation in physical variables is

$$L\bar{k}^5 + (\rho g - \bar{m}\bar{\omega}^2)\bar{k} - \rho\bar{\omega}^2 = 0.$$

When  $\bar{k}$  is small,  $\bar{\omega}$  is also small, giving  $\bar{k}^5 \approx 0$  and  $|\bar{m}\bar{\omega}^2| \ll \rho g$  and hence  $\bar{k} \approx \bar{\omega}^2/g$ . Thus for long wavelengths, and hence long periods, the dispersion equation is the same as for water waves with  $\bar{k} \propto \bar{\omega}^2$  and with no dependence on the ice-sheet thickness or mass density  $\bar{m}$ . When  $\bar{k}$  is large, for typical values of  $\bar{m}$  we find that  $L\bar{k}^5 \gg |(\rho g - \bar{m}\bar{\omega}^2)\bar{k}|$  and hence  $\bar{k} \approx (\rho\bar{\omega}^2/L)^{1/5}$ . Thus for short wavelengths, and hence short periods,  $\bar{k} \propto \bar{\omega}^{2/5}h^{-3/5}$ . The dependence of  $\bar{k}$  on ice sheet thickness comes through the dependence of flexural rigidity on  $h$ , but note that again the effective dispersion equation is not dependent on the ice-sheet mass density.

For each value of  $L$ , the two relations  $\bar{k} \approx \bar{\omega}^2/g$  and  $\bar{k} \approx (\rho\bar{\omega}^2/L)^{1/5}$  are straight lines on a  $\log\bar{k}$  -  $\log\bar{\omega}$  graph which intersect at the point  $\bar{k} = \sqrt[4]{\rho g/L}$  and  $\bar{\omega} = \sqrt[8]{\rho g^5/L}$  (for example see [7] figure 2). The  $\log\bar{k}$  -  $\log\bar{\omega}$  graphs for differing values of  $L$  can be made to coincide by putting the intersection at the common point (1,1) which implies the scaling  $k = \bar{k}l_c$  and  $\omega = \bar{\omega}t_c$  where  $l_c$  and  $t_c$  are the characteristic length and characteristic time, respectively, defined in section 2.2. The resulting graph of scaled roots of the dispersion equation as a function of  $\omega$  for various values of  $L$  is shown in figure 5.

The values of flexural rigidity,  $L$ , are chosen to correspond to ice-sheet thicknesses of  $h = 0.1$  m,  $h = 1$  m, and  $h = 10$  m when the effective Young's modulus takes the typical value of  $5 \times 10^9$  Pa and the density of ice is  $\rho_i = 922.5$  kg m<sup>-3</sup>. The real and imaginary parts of the three roots  $k_T$ ,  $k_D$ , and  $k_E$ , that have non-negative imaginary part, are graphed. Increasing  $k_T$  and  $\text{Im}(k_D)$  (the upper two sets of curves for  $\omega > 2$ ) corresponds to increasing  $h$ , while decreasing values of  $-\text{Re}(k_D)$ ,  $\text{Im}(k_E)$  and  $\text{Re}(k_E)$  (the lower three sets of curves for  $\omega > 2$ ) correspond to increasing  $h$ . Note that the scaling has the effect of making the three curves for the travelling-wave number,  $k_T$ ,

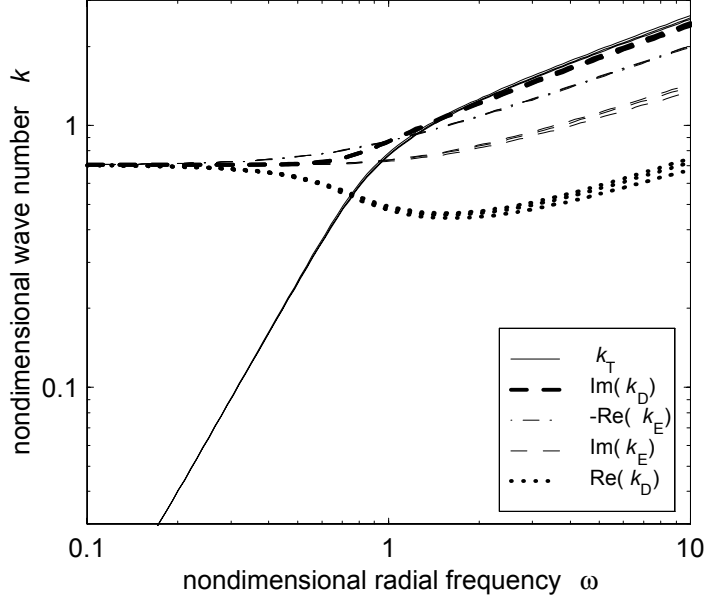


Figure 5: Graph of  $k_T$  (log scale) and the real and imaginary parts of  $k_D$  and  $k_E$  as a function of  $\omega$  (log scale) for three flexural rigidities corresponding to ice thicknesses  $h$  of 0.1, 1 and 10 metres.

very nearly identical for all frequencies, and the curves of the real and imaginary parts of the other roots near to overlapping. Consequently, we can conclude that this scaling to non-dimensional variables has the desirable property of reducing the solutions to a canonical solution depending on  $\omega$  only. Particular physical solutions are found by scaling with respect to characteristic length and time.

Figure 5 also shows that the non-dimensional frequency  $\omega = 1$  sets a transition between distinct regimes in the frequency-wavelength relationship.

When  $\omega \ll 1$  (low frequencies) we have  $k_T \ll \text{Im}(k_D) \simeq -\text{Re}(k_D) \simeq \text{Im}(k_E) \simeq \text{Re}(k_E) \simeq \sqrt{2}$ . Since  $R_T \rightarrow 0$  as  $k_T \rightarrow 0$ , the coefficient of any travelling wave is small and the solution is reduced to the contributions due to the complex roots, which are nearly invariant with frequency. Thus the range  $\omega \ll 1$  has just the single *quasi-static* solution which is essentially the static solution moving in phase with the harmonic loading. Hence, in the quasi-static regime the hydrodynamic forces exerted by the water, given by the term  $\phi_t$  in the linearized Bernoulli equation, may be neglected showing that the restoring force is due to the buoyancy term alone and the water acts as a Winkler foundation.

When  $\omega \gg 1$  (high frequencies),  $k_T$  is no longer small and the solution is *dynamic* since an appreciable travelling wave is generated by the forcing. It is straightforward to show that in this regime  $k_T \simeq |k_D| \simeq |k_E|$  and, as can be seen from figure 5 where the curves have the same slope for  $\omega \gg 1$ , the roots asymptotically approach a given phase. The region  $\omega \approx 1$  sets a range of intermediate behaviour in which the coupling between the load and the ice sheet is greatest.

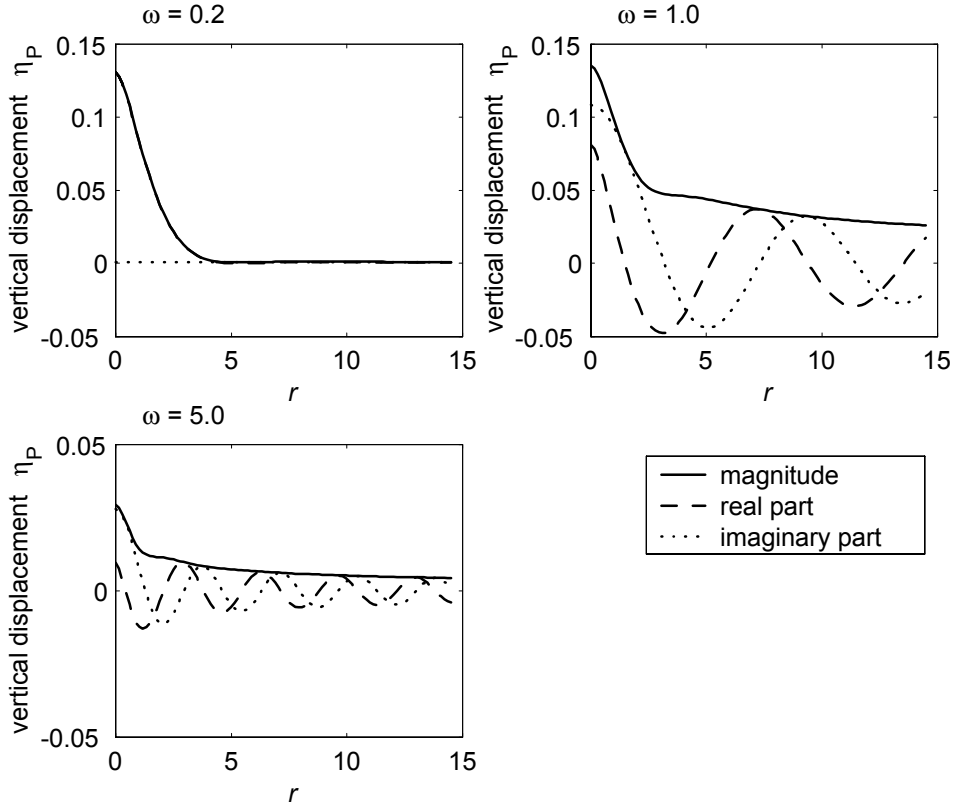


Figure 6: Magnitude, real part and imaginary part of vertical displacement resulting from point forcing at non-dimensional frequencies 0.2, 1.0, and 5.0, when the water is infinitely deep. Responses are shown as a function of non-dimensional distance from the point of forcing.

#### 4.1 Canonical solutions

Plots of canonical solutions for point and line forcing are given in the figures 6 and 7 in the limit of thin ice, or equivalently using the approximation  $m = 0$ .

Figure 6 shows the response to point forcing as a function distance from the forcing,  $r$ , in the low frequency ( $\omega = 0.2$ ), unit frequency, and high frequency ( $\omega = 5.0$ ) regimes. The real and imaginary parts of the solution are shown for infinite water depth, calculated using equation 36. The solutions for the finite depth  $H = 2\pi$ , that could be calculated using equation 23 are visually identical to the graphs shown and so have not been included. That the responses for  $H = \infty$  and  $H = 2\pi$  should be essentially identical is indicated by the displacements at the point of forcing, shown in figure 3, being nearly identical for the depths  $H = \infty$  and  $H = 2\pi$  at all frequencies, in particular the frequencies used here. Note that at low frequencies ( $\omega = 0.2$ ), only the real part of the solution is appreciable and hence the response is in phase with the forcing. In particular, no energy is transferred into the ice on average and no travelling wave is generated. For frequencies above about unit nondimensional frequency ( $\omega \gtrsim 1$ ), the imaginary part of the solution is appreciable, actually larger

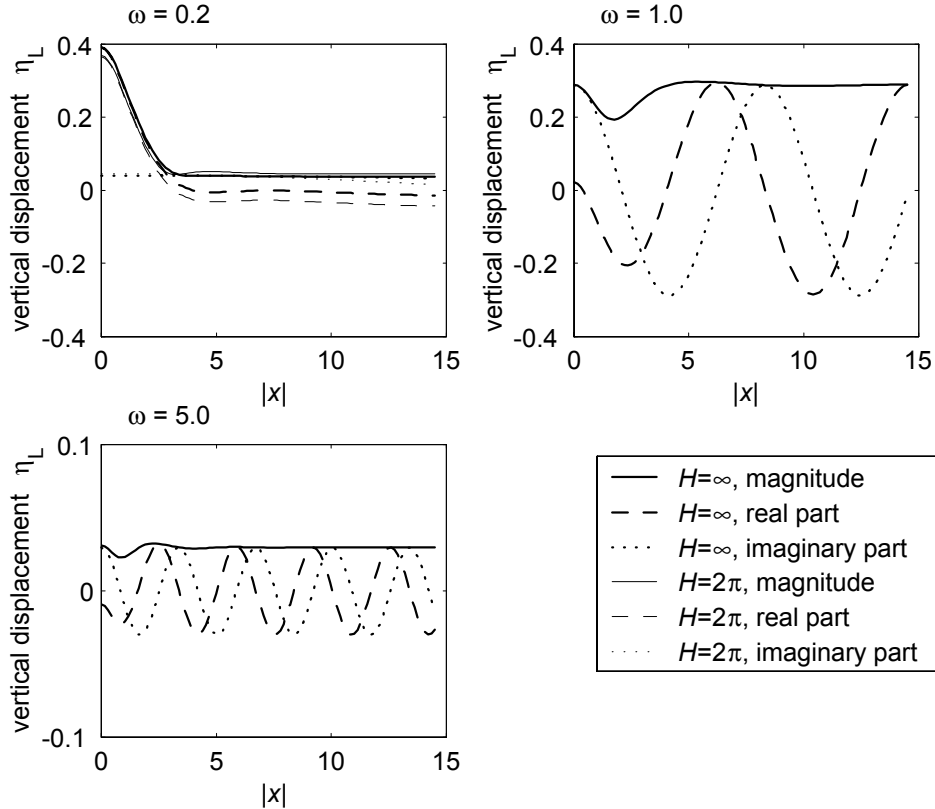


Figure 7: Magnitude, real part and imaginary part of vertical displacement resulting from line forcing at non-dimensional frequencies 0.2, 1.0, and 5.0. For  $\omega = 0.2$  the water depths  $H = 2\pi$  and  $H = \infty$  are shown, while for the other frequencies only the response for  $H = \infty$  is shown. Responses are shown as a function of non-dimensional distance from the point of forcing.

than the real part near the point of forcing, and so energy is transferred into the ice. A travelling wave is generated that carries the energy away, with amplitude being greater for  $\omega = 1$  than  $\omega = 5$ . The amplitude of the travelling wave as a function of frequency is given by the imaginary part of the displacement at  $r = 0$ , which is plotted in figure 3.

Canonical solutions for line forcing are shown in figure 7, also as a function of distance from the line of forcing,  $|x|$ , in the low frequency ( $\omega = 0.2$ ), unit frequency, and high frequency ( $\omega = 5.0$ ) regimes. For line forcing, the solutions in the low frequency regime differ for infinite water depth and for  $H = 2\pi$ , and so the solution for  $H = 2\pi$  and  $\omega = 0.2$  has been included. At the higher frequencies  $\omega = 1.0$  and  $\omega = 5.0$  the solutions for the two depths are visually identical and only the solution for infinite depth, calculated using equation 37 has been plotted. As for the point-forcing case, these similarities and dissimilarities of solutions are indicated by the displacement on the line of forcing graphed in figure 4.

We can conclude from figures 6 and 7 that the depth beyond which the water may be considered to be effectively infinitely deep depends on the nature of the forcing.

For forcing that is localized, that may be treated as a point, non-dimensional water depths greater than  $2\pi$ , i.e. actual depths approximately 6 times the characteristic length, are deep for any rate of forcing. However, for forcing that occurs along a long region, that may be considered a line, the non-dimensional depth  $2\pi$  is not deep, particularly for low rates of applied force. For forcing on a line the water needs to be approximately twice that depth, i.e. actual depths of 12 times the characteristic length, so that the detail of water depth does not affect the response at any rate of forcing.

## 4.2 Other scalings

It is interesting to note that other non-dimensional formulations are possible which do not give a useful reduction to canonical solutions for the range of parameters typical in sea ice dynamics. For example, at very large  $\bar{k}$ ,  $|(\rho g - \bar{m}\bar{\omega}^2)|\bar{k} \gg \rho\bar{\omega}^2$  and  $\bar{m}\bar{\omega}^2 \gg \rho g$  giving the asymptote  $\bar{k} \approx (\bar{m}\bar{\omega}^2/L)^{1/4}$ . Putting the intersection of this relationship and the small- $\bar{k}$  relationship at a common point leads to a different characteristic length and time than derived above. This scaling would be relevant in cases where ice has ten times its actual density, though then the ice sheet would sink. However, this scaling does not have the property of making the wavenumber – frequency graphs overlap for typical mass densities and for periods of geophysical interest, and hence does decouple the dependence of solutions on physical effects and frequency effects.

## 4.3 The approximation $m = 0$

A number of authors omit the mass density of the ice sheet from the plate equation in the system 1, or, equivalently, consider thin ice (ref Goldstien and Marchenko [42]). The graphs of solutions in this paper have also used  $m = 0$ . We now examine the validity of this approximation in the case of infinite water depth.

Figure 8 shows the locus of the three of poles of  $v$  with positive imaginary part, i.e., the wavenumbers  $k_T$ ,  $k_D$ , and  $k_E$ , for the two values of mass density  $m = 0$  and  $m = 0.1$ . On each curve, the magnitude of wavenumber goes from small to large with increasing frequency. The value  $m = 0.1$  is taken as a typical physically-realistic non-dimensional mass density, and corresponds to ice with a Young’s modulus of  $2 \times 10^9$  Pa that is 2.7 m thick. Thinner, or more rigid, ice will have a smaller value of  $m$ . Since  $m \propto (h/E)^{1/4}$ , in fact the values of  $m$  will always be approximately equal to 0.1, except for extreme cases.

As can be seen in figure 8, there is a difference in the positions of the poles between  $m = 0$  and  $m = 0.1$ , particularly at higher frequencies (greater magnitude of wavenumber). However, the graphs of canonical solutions using  $m = 0.1$  are qualitatively unchanged from the solutions using  $m = 0$ . The primary difference in responses is a decrease in the wavelength of the travelling wave with increasing  $m$ , as can be seen by the slight increase in wavenumber marked for  $\omega = 0.1$ ,  $\omega = 1.0$ , and  $\omega = 10$  in figure 8, or in figure 5. The same decrease in wavelength occurs, to first order, by setting  $m = 0$  and increasing frequency by the multiplicative factor

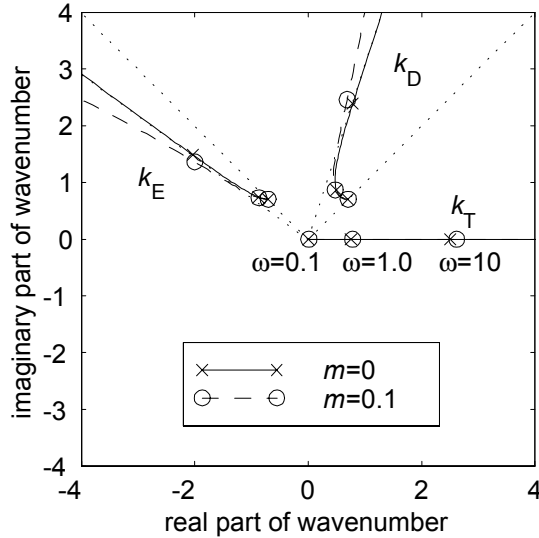


Figure 8: Locus of poles of  $v(k)$  with positive imaginary part for  $m = 0$  and  $m = 0.1$ . The poles for  $\omega = 0.1, 1.0$ , and  $10$  are marked in each case; the magnitude increasing with frequency. The lines from the origin with angle  $\pi/4, \pi/5, 3\pi/4$ , and  $4\pi/5$  are shown for reference.

$(1 + mk_T/2)$ . Thus, the response for ice sheets with non-zero mass density lies within the range of behaviour exhibited by solutions using  $m = 0$ . However the detail of the frequency-wavelength relationship is altered by this approximation, since a given wavelength near maximum coupling actually occurs at roughly 5% lower frequency than is predicted using  $m = 0$ . Since this difference is easily measurable, the mass density needs to be included when interpreting experimental measurements. However, as  $m$  is not strongly dependent on ice properties, and the dependence of solutions on  $m$  is weak, a reasonable estimate of  $m$  allows accurate calculation of the characteristic length.

Dotted lines with angle  $\pi/4, 2\pi/5, 3\pi/4$ , and  $4\pi/5$  are shown in figure 8 for reference. We see that when  $m = 0$  the phase of  $k_D$  lies between  $\pi/4$  and  $2\pi/5$  with the lower limit occurring when  $\omega = 0$  and the upper limit being the asymptotic value as  $\omega \rightarrow \infty$ . Similarly, the phase of  $k_E$  increases from  $3\pi/4$  at  $\omega = 0$  monotonically to  $4\pi/5$  as  $\omega \rightarrow \infty$ . In particular, note that the poles, including those with negative imaginary part, make a square diamond pattern at low frequencies ( $k_T \rightarrow 0$  as  $\omega \rightarrow 0$ ) and a regular pentagon at high frequencies. These are the quasi-static and dynamic regimes described previously. In the case  $m > 0$ , the phase of the roots  $k_D$  and  $k_E$  exceeds  $2\pi/5$  and  $4\pi/5$ , respectively, at high frequencies. It can be shown that the phase equals these angles at  $\omega = 1/\sqrt{m}$ . However, as noted above, there is no qualitative change in the responses and this increase in asymptotic phase does not seem to be physically important.

## 5 Conclusions

We have derived analytic expressions for the dynamic flexural response of a floating plate and floating beam when loaded at a point. The expressions giving responses for finite water depth are each infinite sums over natural modes of the system, which may be truncated to allow accurate computation. In the case of infinite water depth the expressions simplify further to the sum of standard special function summed over three roots of the fifth-order polynomial that is the analytically-continued dispersion equation. The computation of those solutions is virtually trivial.

The responses are given in non-dimensional form, thereby reducing the number of solutions required to show the full range of behaviour of floating plates and beams. The scaling to non-dimensional form is itself an important result since it is the scaling that allows straightforward categorizing of the regimes of physical behaviour according to non-dimensional frequency. We found that the response was quasi-static at low frequencies and dynamic, with travelling waves generated, at high frequencies. Maximum coupling between the loading and the ice sheet occurs just below unit non-dimensional frequency in the transition between the two regimes. Further, since this scaling depends only on the structure of the dispersion equation, and not on the nature of forcing, the same scaling will give reduction to canonical solutions for other dynamic problems involving fluid-loaded plates.

## Acknowledgements

The authors are grateful to the Royal Society of New Zealand for financial support in the form of a Marsden grant. This work has in part been undertaken within the LOLEIF project in the framework of the EU-sponsored Marine Science and Technology (Mast III) Programme under contract number MAS3-CT97-0078. We warmly thank John Dempsey for useful and encouraging criticism throughout this work.

## References

- [1] Squire, V. A., Robinson, W. H., Langhorne, P. J. and Haskell, T. G., 1988 Vehicles and aircraft on floating ice, *Nature* 133, N0. 6169 159-161.
- [2] Crighton, D. G. (1998) Fluid loading: the interaction between sound and Vibration, *Proc. I. O. A.* 10 part 2, 1-35.
- [3] Forbes, L. K. 1986 Surface waves of large amplitude beneath an elastic sheet. 1. High-order series solution. *J. Fluid Mech.* 169, 409-428.
- [4] Forbes, L. K. 1988 Surface waves of large amplitude beneath an elastic sheet. 2. Galerkin solution. *J. Fluid Mech.* 188, 491-508.
- [5] Fox, C., & Squire, V.A. 1991 Coupling between the ocean and an ice shelf. *Annals Glaciol.* 15, 101-108.

- [6] Fox, C. 1992 Large amplitude sea/ice coupling. In *Advances in Ice Technology: Proc. of the Third Int. Conf. on Ice Technology, 11-13 August 1992, Cambridge, MA, USA* (ed. T. K. S. Murthy, W. M. Sackinger & P. Wadhams), pp. 293-304. Computational Mechanics Publications.
- [7] Fox, C., & Squire, V.A. 1994 On the Oblique Reflexion and Transmission of Ocean Waves at Shore Fast Sea Ice. *Phil. Trans. R. Soc. Lond. A* (1994) **347**, 185-218.
- [8] Langhorne, P. J., Squire, V. A., Fox, C. and Haskell, T. G. Role of fatigue in wave-induced break-up of sea ice: A review, in *Ice In Surface Waters*, vol. 2, Hung Tao Shen ed., 14th International Symposium on ice, Potsdam/New York/USA 27-31 July 1998, pp1019-1023.
- [9] Fox, C. and Chung, H. 1998 Green's Function for Forcing of a Thin Floating Plate, Department of Mathematics Research Report Series number 408, ISSN 1173-0889, The University of Auckland. Available at <http://math.auckland.ac.nz>.
- [10] Greenhill, A. G. 1887 Wave motion in hydrodynamics. *Am. J. Math.* 9, 62-112
- [11] Kerr, A.D. & Palmer, W.T. 1972 The deformations and stresses in floating ice plates. *Acta mech.* **15**, 57-72.
- [12] Mindlin, R. D. 1951 Influence of rotatory inertia and shear on flexural motions of isotropic, elastic plates. *Journal of Applied Mechanics* Vol. 18 (1951) 31-38.
- [13] Nevel, D. E., 1970 Vibration of a floating ice sheet, U.S. Army Cold Regions Research and Engineering Laboratory report No. RR 281.
- [14] Doronin, Yu. P. and Kheisin, D. E. (1977) *Sea Ice*, New Dehli, Amerind Publishing Co. Pvt. Ltd..
- [15] Hertz, H. 1884 Über das Gleichgewicht schwimmender elastischer Platten, *Annalen der Physik und Chemie*, 22, no. 7, (1884) 449-455.
- [16] John, Fritz (1949) On the motion of floating bodies. I. *Communications in pure and applied mathematics*, **2**, 13-57.
- [17] John, Fritz (1950) On the motion of floating bodies. II. Simple harmonic motions. *Communications in pure and applied mathematics*, **3**, 45-101.
- [18] Johnson, Johnny R. and Johnson, David E. (1975) *Linear systems analysis*, The Ronald Press Company, New York.
- [19] Kheisin, D. Ye. 1967 Dynamics of ice cover, *Gidrometeorologicheskoe Izdatel'stvo*, Leningrad, USSR. English translation available as U.S. Army Foreign Science and Technology Centre technical translation FSTC-HT-23-485-69.

- [20] Marchenko, A. V. (1997) Resonance interactions of waves in an ice channel, *J. Appl. Maths Mechs*, **61** No. 6, 931-940.
- [21] Pavlov, B. (1996) Splitting of acoustic resonances in domains connected by a thin channel. *New Zealand Journal of Mathematics*, **25** number 2, 199-216.
- [22] Westergaard, H. M. 1926 Stresses in concrete pavements computed by theoretical analysis, *Public Roads*, 7, (1926) 25-35.
- [23] Squire, V. A., Rottier, P. and Fox, C. 1994 A first look at some wave-ice interaction data from McMurdo Sound, Antarctica. In *Sea Ice Observations and Modelling – Proceedings of the 93's International Symposium on Sea Ice*. Y. Zhouwen, C.L. Tang, R.H. Preller, W. Huiding eds. China Ocean Press, Beijing, PRC (1994) 19-33.
- [24] Stadler, W. and Shreeves, R. W., (1970) The transient and steady-state response of the infinite Bernoulli-Euler beam with damping and an elastic foundation, *J. Mech. and Appl. Math.* vol. 33 (May 1970), pp 197-208.
- [25] Stadler, W. (1971) The general solution of the classical problem of the response of an infinite plate with an elastic foundation and damping, *Journal of Elasticity*, vol. 1 (1971) pp 37-49.
- [26] Sneddon, I. N. (1944) The symmetrical vibrations of a thin elastic plate. *Proceedings of the Cambridge Philosophical Society* **41** 27-43.
- [27] Sneddon, I. N. (1951) *Fourier transforms*. McGraw-Hill, New York, 1951.
- [28] Dempsey, J. P., Zhao, Z. G. and Li, H., (1991) Axisymmetric indentation of an elastic layer supported by a Winkler foundation, *Int. J. Solids Structures*, vol. 27, no. 1, pp 73-87.
- [29] Zhao, Z. G. and Dempsey, J. P. (1996) Planar forcing of floating ice sheets, *Int. J. Solids Structures*, vol 33, n0 1, pp 19-31.
- [30] Dempsey, J.P. and Z.G. Zhao (1993) Elastohydrodynamic response of an ice sheet to forced sub-surface uplift. *Journal of the Mechanics and Physics of Solids* Vol.41 (1993) 487-506.
- [31] Bracewell, Ron 1965 *The Fourier Transform and its Applications*. McGraw-Hill, New York.
- [32] Stakgold, Ivar 1967 *Boundary Value Problems of Mathematical Physics*, vol. 1, The Macmillan Company, New York.
- [33] Strathdee, J., Robinson, W. H., and Haines, E. M., *Moving loads on ice plates of finite thickness*, *J. Fluid Mech.* (1991) **226**, 37-61.
- [34] Duffy, D. G. *The response of floating ice to a moving, vibrating load*. *Cold Regions Science and Technology*, **20** (1991) 51-64.

- [35] Abramowitz, M. & Stegun, I.A. 1972 *A Handbook of Mathematical Functions*. Dover Publications, New York.
- [36] Wyman, Max. 1950 Deflections of an Infinite Plate, *Canadian Journal of Research*, **28**, sec. A, 293-302.
- [37] Fox, C., Wilcocks, L. and Haskell, T. 1996 A Calculation of Sea-Ice Young's Modulus Using Under-Ice Pressure Measurements. Dept. Math. Report 335, The University of Auckland, ISSN 1173-0889.
- [38] Erdélyi, A. (ed.) 1954, *Tables of integral transforms*, vol. 1, 1.2(11), California Institute of Technology, Bateman Manuscript Project, McGraw-Hill, New York.
- [39] Fox, C., & Squire, V.A. 1990 Reflexion and Transmission characteristics at the edge of shore fast sea ice. *J. geophys. Res.* **67**, 4531-4547.
- [40] Wehausen, J. V. and Latoine, E. V. 1960 Surface Waves in Handbuch der Physik, volume 9, Springer Verlag, Berlin.
- [41] Roos, B. W. 1969 *Analytic functions and distributions in physics and engineering*. John Wiley and Sons, Inc.
- [42] Goldshtein, R. V. and Marchenko, A. V. 1989 The diffraction of plane gravitational waves by the edge of an ice cover. *Prikl. Matem. Mekhan.* **53**, No. 6. 731-736.